Characterization, Electrical and Electrochemical Study of $La_{0.9}Sr_{1.1}Co_{1-x}Mo_xO_4$ ($x \leq 0.1$) as Cathode for Solid Oxide Fuel Cells

T. GHORBANI-MOGHADAM,[1] A. KOMPANY,[1,2,5]
M.M. BAGHERI-MOHAGHEGHI,[3] M. EBRAHIMIZADEH ABRISHAMI,[2]
and M. GOLMOHAMMAD[4]

1.—Materials and Electroceramics Lab, Department of Physics, Ferdowsi University of Mashhad, Mashhad, Iran. 2.—Nano Research Center, Ferdowsi University of Mashhad, Mashhad, Iran. 3.—School of Physics, Damghan University, Damghan, Iran. 4.—Renewable Energy Department, Niroo Research Institute, Shahrak Gharb, Tehran, Iran. 5.—e-mail: kompany@um.ac.ir

In this study, Ruddlesden–Popper $La_{0.9}Sr_{1.1}Co_{1-x}Mo_xO_4$ ($x \leq 0.1$) powders were successfully synthesized using a modified sol–gel method. The structural analysis revealed that all samples had a tetragonal phase at room temperature. The electrical conductivity measurements showed that all samples had semiconducting behavior in the range of room temperature to 850°C. Moreover, it was found that the electrical conductivity of the ceramics was enhanced with the increase of Mo doping, at temperatures higher than 300°C up to 850°C. This enhancement of the electrical conductivity can be due to Co^{3+}–O–Mo^{5+}–O–Co^{2+} double-exchange interaction. The EIS measurements of the symmetrical cells were carried out for $x = 0$, 0.03 and 0.1 samples at 650°C, 750°C and 850°C. The obtained area specific resistance (ASR) values of $La_{0.9}Sr_{1.1}Co_{1-x}Mo_xO_4$ on ceria-gadolinium oxide (CGO) electrolyte at 850°C were 0.36 Ω cm^2, 0.35 Ω cm^2 and 1 Ω cm^2 for samples $x = 0$, 0.03 and 0.1, respectively. These results indicate that the electrical conductivity of pure sample ($La_{0.9}Sr_{1.1}CoO_4$) has been enhanced by Mo substitution in Co ion sites, but limits the oxygen ion transport.

Key words: Layered compounds, modified sol–gel, electrochemical impedance spectroscopy (EIS), electrical properties, electrochemical performance

INTRODUCTION

In order to improve the performance of solid oxide fuel cells (SOFCs), it is essential to develop new materials having good cathodic behavior including high electrical and electrochemical properties along with high thermal and chemical stabilities. Many efforts have been made based on mixed ionic and electronic conductor (MIEC) compounds to achieve these goals.[1–5] A number of researchers have replaced certain cations in A or B sites of ABO_3 perovskites, mostly in Co- and Fe-based compounds. In these compounds, oxygen vacancy can improve the oxygen reduction reaction kinetics for SOFC applications. Recently, doping perovskites based on transition metals, with high-charge-valency cations, such as Nb^{5+}, Ta^{5+}, Sb^{5+}, W^{6+} and Mo^{6+} have attracted much attention.[6–9] The pioneering work was carried out by partial substitution of these cations at Co ion sites in $SrCoO_3$-based compounds which improved their structural stability at high temperatures.[10–15] The phase structure of $SrCoO_3$ is hexagonal at room temperature and changes to tetragonal at temperatures higher than 500°C. According to the work by Aguadero et al.,[11] the partial substitution (< 0.1) of Co ion sites in $SrCoO_3$

with high-charge-valency cations stabilized the tetragonal phase structure over the whole range of measured temperatures (30–700°C). In addition, they found that the electrical and electrochemical activities of their samples were improved by reducing Co^{4+} to a Co^{3+} population and enhancement of Co^{3+}–O^{2-}–Co^{4+} double-exchange interactions. Demont et al. investigated the effect of doping Mo in $Ba_{0.5}Sr_{0.5}Co_{0.8}Fe_{0.2}O_3$ (BSCF) compound.[16] They reported that the increase of electrical conductivity in this compound is due to the formation of a double-perovskite structure inducing two paths for electron conduction through MoO_6 and CoO_6 sublattices. Also, it has been reported that low dopant content of molybdenum ($x = 0.02$) improved the structural phase stability of BSCF compounds.[17] Furthermore, it has been found that the perovskite materials based on Mo cations such as $SrMoO_3$ have high electrical conductivity (10^4 S/cm) and good electrochemical performance for SOFC applications at room temperature.[18] However, the ionic conductivity of these oxides is not high enough, due to the lack of oxygen vacancies. The high electrical and electrochemical activities of these materials have made them promising candidates as new cathode materials.[19–21] In cobalt-based compounds, such as $Sr_2Co_{1+x}Mo_{1-x}O_6$ double perovskite, the thermal expansion coefficient (TEC) was found to decrease remarkably by introducing molybdenum, showing the best performance as a cathode/anode symmetrical cell in SOFCs.[22]

However, to the best of our knowledge, Mo-doped Ruddlesden–Popper cobalt-based compounds, as cathode materials for SOFCs, have not been studied. In this research, the effects of partial substitution of Mo in Co ion sites on structural, electrical and electrochemical properties of $La_{0.9}Sr_{1.1}CoO_4$ have been investigated.

EXPERIMENTAL PROCEDURES

Synthesis

Compounds of $La_{0.9}Sr_{1.1}Co_{1-x}Mo_xCoO_4$ ($x = 0$, 0.03, 0.05, 0.07 and 0.1) were synthesized using a modified sol–gel method.[23] The starting materials were $La(NO)_3.6H_2O$, $Co(NO_3).6H_2O$, $Sr(NO_3)_2$ and $(NH_3)_6Mo_7O_{24 \cdot 1.5}H_2O$. The precursors, with proper stoichiometric proportions, were dissolved in deionized water under stirring at room temperature. At the same time, gelatin, as the polymerization and stabilization agent, was dissolved separately in deionized water at 60°C under stirring for 30 min. Then, the prepared ionic solution was gradually added to the aqueous solution of gelatin while stirring at 80°C in an oil bath. The obtained resin was heated at 220°C for 2 h, and the resulting black powder was then ground and calcined at 1100°C for 6 h.

Characterization Methods

In order to study the structure and lattice dynamics of the synthesized $La_{0.9}Sr_{1.1}Co_{1-x}Mo_xCoO_4$, x-ray diffraction (XRD) and high temperature x-ray diffraction (HT-XRD) spectroscopy (x-ray diffractometer: GNR, Explorer, CuKα, $\lambda = 1.5406$ Å), and infrared transmittance spectra, in the range of 200–700 cm^{-1}, were recorded using Fourier transform infrared (FTIR) spectroscopy (standard PerkinElmer spectrum: 400MIR/FIR spectrometer). The magnetic characterization of the samples was carried out using a vibrating-sample magnetometer (VSM) technique at room temperature. In order to measure the electrical conductivity of the prepared samples, a four-point DC method was used in the range of room temperature to 850°C in an air environment.[24,25] The synthesized powders were first pressed into pellets and then sintered at 1100°C for 10 h. The electrochemical activity of the samples as cathodes was studied using electrochemical impedance spectroscopy (EIS) with a potentiostat/galvanostat (Autolab 302N) at high stability conditions, in the frequency range of 10 Hz to 1 MHz at 650°C, 750°C and 850°C. Ceria gadolinium oxide (CGO) powder was first pressed into pellets and then sintered at 1350°C for 4 h in air to obtain a dense electrolyte substrate. $La_{0.9}Sr_{1.1}Co_{1-x}Mo_xO_4$ ($x = 0.03$ and 0.07) slurry was screen-printed on both sides of the prepared CGO electrolyte to form a symmetrical cell which was then heated at 1200°C for 4 h. The thickness of the cathode layers was about 30 μm, and silver meshes were used as the current collectors on both sides of the cells.

RESULTS AND DISCUSSION

Structural: XRD and FTIR Analyses

The XRD patterns of $La_{0.9}Sr_{1.1}Co_{1-x}Mo_xO_4$ ($x = 0$, 0.03, 0.05, 0.07 and 0.1) synthesized powders are presented in Fig. 1 which shows that the crystal structure of all samples is tetragonal, with the space group I4/mmm. The HT-XRD of $La_{0.9}Sr_{1.1}Co_{1-x}Mo_xO_4$ sample pattern at maximum measuring temperature (850°C) and the maximum dopant content ($x = 0.1$) shows that the tetragonal structure is stable without any significant secondary phases (Fig. 2). The calculated lattice parameters at room temperature are given in Table I. As reported earlier,[23] the Co valence in $La_{0.9}Sr_{1.1}CoO_4$ is 3.06, and the spin state of the Co^{3+} ions is a mix of the intermediate- (IS: 0.56 Å) and low-spin states (LS: 0.54 Å). Although the ionic radii of Mo ions are 0.61 Å and 0.59 Å for Mo^{5+} and Mo^{6+} in octahedral coordination,[11,17,26] the c parameter is slightly decreased with the increase of Mo content (Table I). This can be due to the substitution of Co^{3+}(IS) by

Mo^{5+}/Mo^{6+} and, consequently, the reduction of the $Co^{3+}(IS)$ population, as confirmed by the Fourier transform far-infrared (FT-FIR) spectra. The FT-FIR spectra of the synthesized samples, in the range of $200-700$ cm^{-1}, are presented in Fig. 3. Also, the

vibration mode data are given in Table II. From Fig. 3 and Table II, it can be seen that the shift of wavenumbers corresponding to La/Sr–O(II)–Co and Co–O(I) vibration modes are more pronounced with Mo doping, compared to the other modes. The vibration mode splitting of La/Sr–O(II)–Co, which occurs in $La_{2-x}Sr_xCoO_4$ for $x = 1.1$ and 1.3, is believed to be a result of increasing Co^{3+} (IS) population and the appearance of Jahn–Teller distortion.[23] As shown in Fig. 3, this splitting gradually disappears with increasing Mo, indicating that the different amounts of Mo doping affect the Co^{3+} spin sate of $La_{0.9}Sr_{1.1}CoO_4$. In addition, the wave number of the La/Sr–O(II)–Co vibration mode increased from 513 cm^{-1} for $x = 0–534$ cm^{-1} for $x = 0.1$. This wavenumber enhancement reveals that the increase of Co–O(II) covalent bond strength corresponds to the elimination of Jahn–Teller elongation along the c axis.
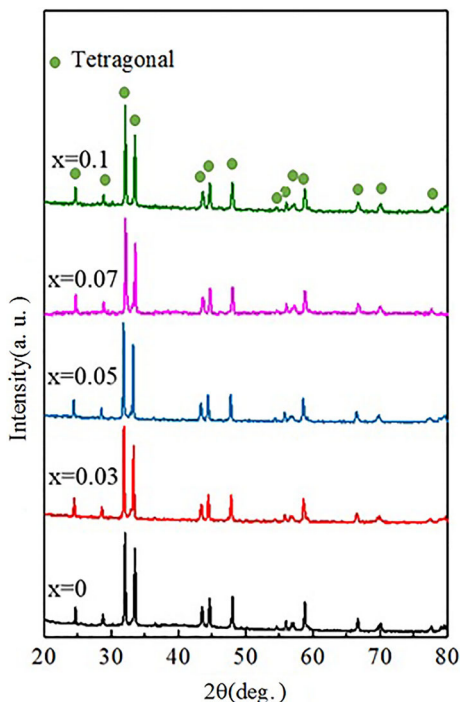

Fig. 1. XRD patterns of $La_{0.9}Sr_{1.1}Co_{1-x}Mo_xO_4$ $(x = 0, 0.03, 0.05, 0.07, 0.1)$ at room temperature.
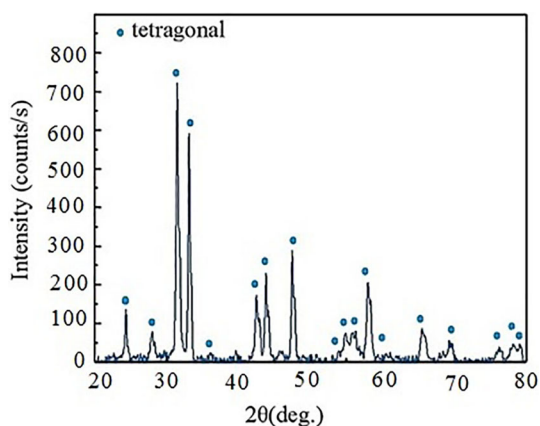
Fig. 2. HT-XRD pattern of $La_{0.9}Sr_{1.1}Co_{0.9}Mo_{0.1}O_4$ at 850°C.
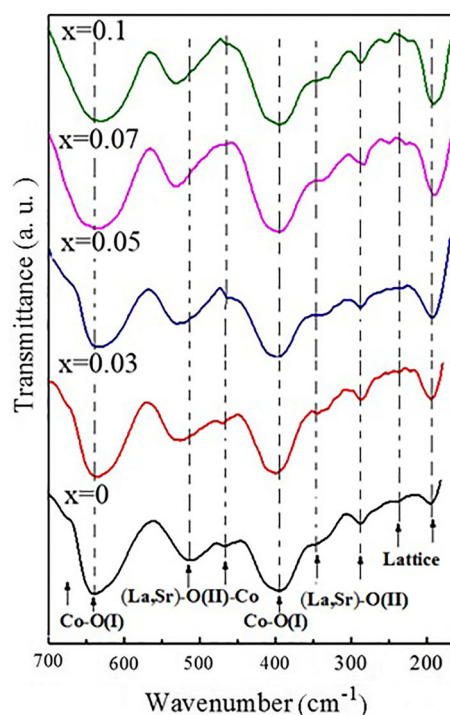
Fig. 3. FTIR spectra of $La_{0.9}Sr_{1.1}Co_{1-x}Mo_xO_4$ $(x = 0, 0.03, 0.05, 0.07, 0.1)$ at room temperature.

Table I. The lattice parameters of the synthesized $La_{0.9}Sr_{1.1}Co_{1-x}Mo_xO_4$ powders

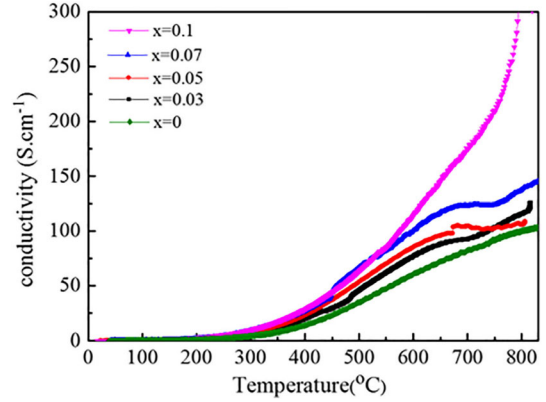|	X = 0	X = 0.03	X = 0.05	X = 0.07	X = 0.1
a (Å)	3.803	3.807	3.808	3.806	3.801
c (Å)	12.510	12.512	12.518	12.492	12.481
V (Å3)	180.997	181.370	181.530	180.670	180.510

Table II. The wavenumbers (cm^{-1}) and the assignments of FT-FIR bands of the synthesized La$_{0.9}$Sr$_{1.1}$Co$_{1-x}$Mo$_x$O$_4$ powders

Symmetry	X = 0	X = 0.03	X = 0.05	X = 0.07	X = 0.1	Assignment
E$_u$	641	637	635	633	630	Co–O(I)–Co stretching
A$_{2u}$	513 and 468	527 and 469	530 and 467	530 and 465	534	La/Sr–O(II)–Co stretching
E$_u$	397	403	405	400	400	Co–O(I)–Co deformation
A$_{2u}$	340	338	340	340	340	La/Sr–O(II) deformation
E$_u$	286	286	286	286	286	La/Sr–O(II) stretching
A$_{2u}$	236	239	242	247	250	Lattice distortion
E$_u$	194	197	200	227	226	Lattice distortion
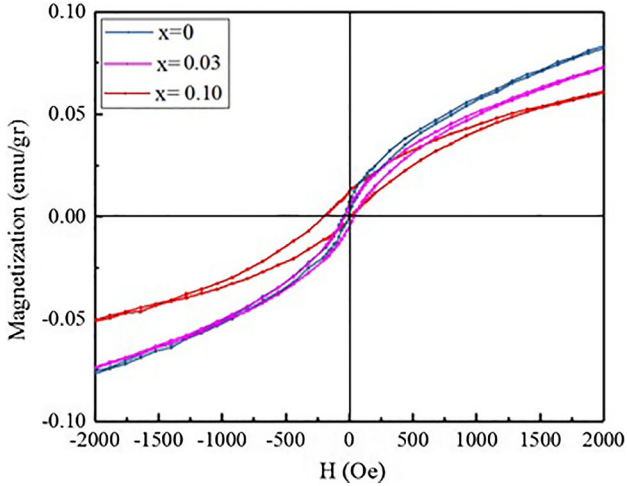
Fig. 4. Magnetic hysteresis loops of La$_{0.9}$Sr$_{1.1}$Co$_{1-x}$Mo$_x$O$_4$ (x = 0, 0.03, 0.1) at room temperature.

Fig. 5. Electrical conductivity of the sintered La$_{0.9}$Sr$_{1.1}$Co$_{1-x}$Mo$_x$O$_4$ ceramics in the range of room temperature to 850°C.

Magnetic Properties: VSM Analysis

The magnetic hysteresis loops of La$_{0.9}$Sr$_{1.1}$Co$_{1-x}$Mo$_x$O$_4$ (x = 0, 0.03 and 0.1) powders, obtained at room temperature, are shown in Fig. 4. As can be seen, for the sample with x = 0, the magnetization (M) has increased sharply with the increase of the magnetic field (H). However, because of the coexistence of both ferromagnetic (FM) and antiferromagnetic (AFM) behaviors, the saturation has not occurred. The observed FM behavior in the undoped sample originates from the double-exchange interaction between Co^{4+} and Co^{3+}. Mo doping has decreased the magnetization value, and the AFM behavior is more significant than the FM behavior, which can be due to the Co^{3+}–O–Co^{3+} super-exchange interaction. In fact, the high valence (+5 and +6) of Mo cations decreases the Co^{4+}/Co^{3+} ion ratio and in turn reduces the double-exchange interaction of Co^{4+}–O–Co^{3+}. For the x = 0.1 sample, the antiferromagnetic characteristic is more dominant, and the coercive field (Hc) is rather large. This can be related to the magnetic inhomogeneity states which cause the large blocking wall motion of La$_{0.9}$Sr$_{1.1}$Co$_{0.9}$Mo$_{0.1}$O$_4$.[27]

Electrical Properties

The electrical conductivity of all samples, as a function of temperature, was measured in the range of room temperature to 800°C. As can be seen in Fig. 5, the electrical conductivity has increased with the increase of Mo doping contents, above 300°C. All samples showed semiconducting behavior in the whole range of measured temperature. The maximum conductivity found was 300 S/cm for the sample with x = 0.1 at around 800°C. Our Mo-doped samples have higher electrical conductivity compared to some other $R - P$ materials such as manganite compounds, La$_{2-x}$Sr$_x$MnO$_4$,[28] La$_{1.2}$Sr$_{0.8}$Mn$_{0.4}$Fe$_{0.6}$O$_4$,[29] and nickelate compounds, La$_{2-x}$Sr$_x$NiO$_4$.[30,31] The electrical conductivity enhancement in our samples can be due to electron hopping between the 4d orbital of Mo^{5+} and the 3d orbital of Co^{3+} cations, similar to that reported by Cowin et al.[32] for Mo-doped SrCaFe$_{1-x}$Mo$_x$O$_6$ double perovskites. According to their results, the 3d^5(t$_{2g}^3$ e$_g^2$) orbitals of Fe have similar energy level to the 4d^1(t$_{2g}^1$) orbital of Mo which forms a narrow conduction band, leading to metallic behavior. Also, they reported that in a delocalized Fe^{3+}–Mo^{5+} configuration, the 3d^5 orbitals of Fe electrons are localized, while 4d^1 orbitals of Mo electrons are itinerant. They concluded that electron hopping from the 4d^1 orbital of Mo through the O-2p orbitals to the empty states of the t_{2g} orbital of Fe leads to the double-exchange mechanism in the form of Fe^{3+}–O–Mo–O–

Fe^{2+} interaction. Itoh et al.[33] studied the electrical and magnetic properties of Sr$_2$CoMoO$_6$ and reported the occurrence of hybridization between Mo(4d) and Co(3d). Also, the appearance of semiconducting and antiferromagnetic behaviors in their sample can be related to hybridization between Co^{2+}(t_{2g}^5 e$_g^2$) and Mo^{6+}(4d^0) cations. Regarding these results, the electrical conductivity enhancement with the increase of Mo doping contents in our work can be due to the electron hopping in the form of Co^{3+}–O–Mo^{5+}/Mo^{6+}–O–Co^{2+} double-exchange interaction. Arrhenius plots of our samples are presented in Fig. 6. As can be seen in this figure, the plots are linear in the range of 400–800°C for both undoped and Mo-doped samples. This can be due to the contribution of a small polaron hopping mechanism which occurs at these temperatures.[34] The calculated activation energies are obtained as 0.345 eV, 0.340 eV, 0.376 eV, 0.382 eV and 0.387 eV for the samples with x = 0, 0.03, 0.05, 0.07 and 0.1, respectively. SEM images of La$_{0.9}$Sr$_{1.1}$Co$_{1-x}$Mo$_x$O$_4$ sintered ceramics (for x = 0, 0.03 and 0.1) after performing the electrical measurements are given in Fig. 7. These micrographs are taken from the surface of the ceramics, after electrical measurements. The high porosity of the doped samples in comparison with the pure one, can be due to the increase of losing oxygen at the surface during the electrical measurement. These microstructures are also observed in a SiMo cast iron sample, which has an oxide layer in the surface.[35]

Electrochemical Performance

The electrochemical performance of La$_{0.9}$Sr$_{1.1}$Co$_{1-x}$Mo$_x$O$_4$ (x = 0, 0.03 and 0.1), according to the EIS data, from a symmetrical cell of cathodes in oxygen at 650°C, 750°C and 850°C, is given in Fig. 8. In this figure, the polarization resistance value (R_p) is the distance interceptions between low and high frequencies with the real axis.[36] This polarization resistance is mainly due to the adsorption, diffusion and oxygen ion transport in the cathode. As shown in Fig. 8, the value of R_p
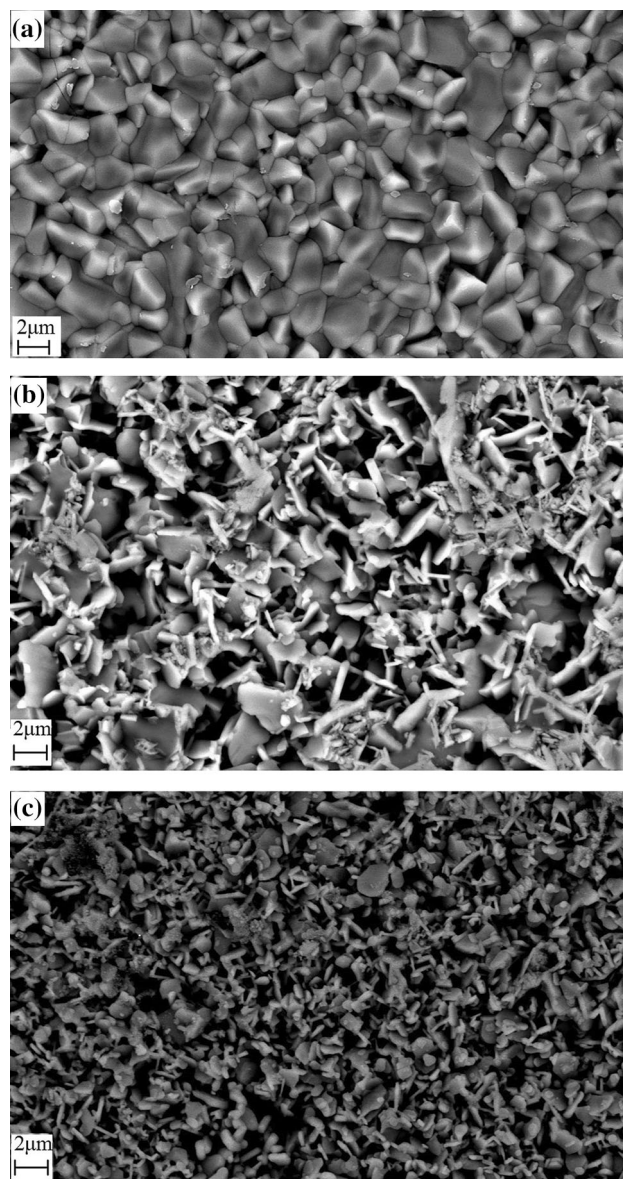

Fig. 7. SEM micrographs of La$_{0.9}$Sr$_{1.1}$Co$_{1-x}$Mo$_x$O$_4$ sintered ceramics for (a) x = 0, (b) x = 0.03 and (c) x = 0.1 after electrical measurements.

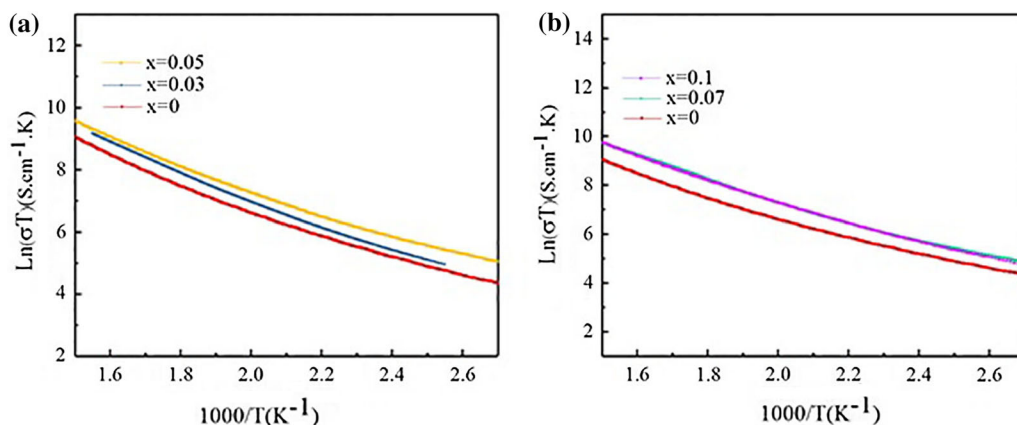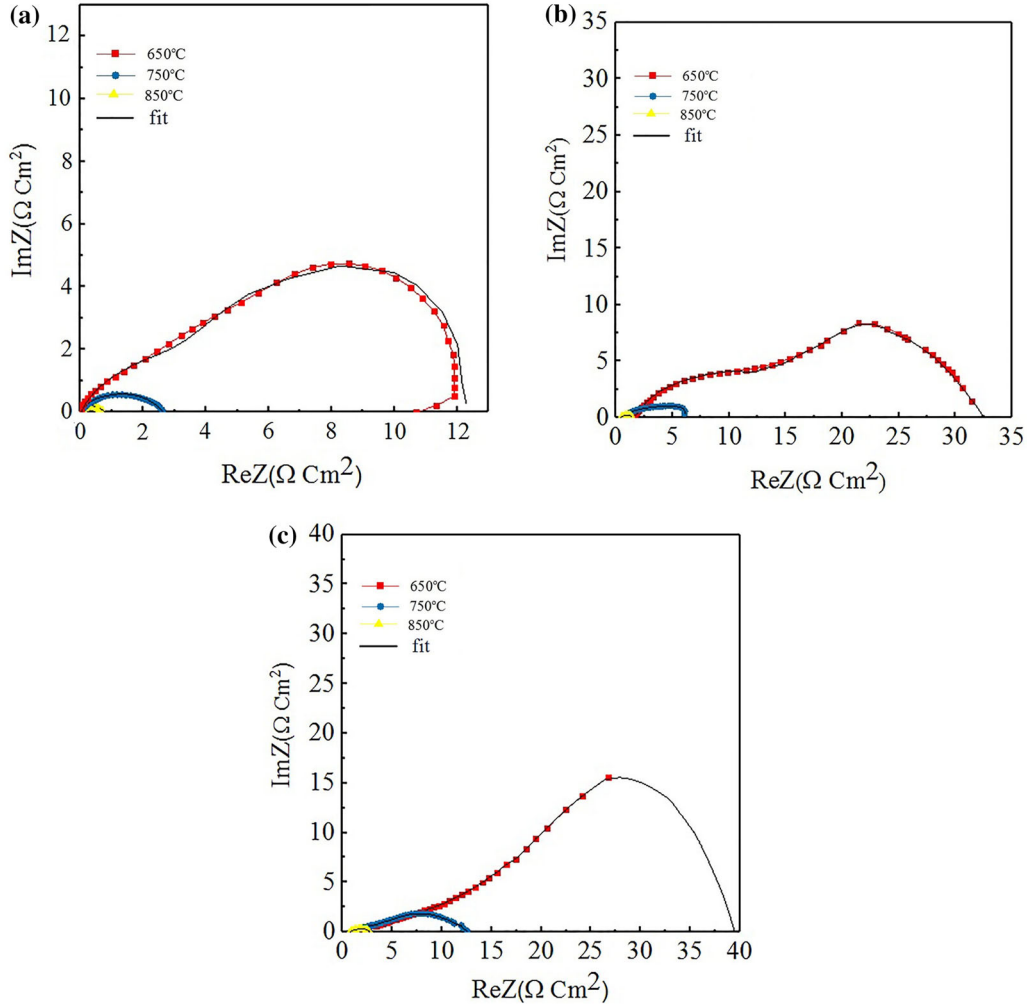Fig. 6. Arrhenius plots of La$_{0.9}$Sr$_{1.1}$Co$_{1-x}$Mo$_x$O$_4$ electrical conductivity for (a) x = 0, 0.03, 0.05 and (b) 0.07, 0.1.

Fig. 8. Impedance spectra of the cathodic symmetrical cell of $La_{0.9}Sr_{1.1}Co_{1-x}Mo_xO_4$ (a) $x = 0$, (b) $x = 0.03$ and (c) $x = 0.1$ compounds, measured at 650°C, 750°C and 850°C.

Table III. The equivalent circuit data obtained from the cathodic symmetrical cell of $La_{0.9}Sr_{1.1}Co_{1-x}Mo_xO_4$ at three different temperatures (unit of R: $\Omega\ cm^2$)

Temperature	$x = 0$		$x = 0.03$		$x = 0.1$	
	R_{ct}	R_{nct}	R_{ct}	R_{nct}	R_{ct}	R_{nct}
650°C	4.5	7.8	12.5	18.9	4.6	39.5
750°C	2.5	0.15	1.68	4.58	1.72	9.16
850°C	0.61	0.05	0.23	0.81	0.85	1.42

decreases with increasing temperature, showing the semiconducting behavior of the samples. The area specific resistance (ASR) for the sample with $x = 0.03$ is 0.35 $\Omega\ cm^2$ which is very close to the value for the pure sample (0.36 $\Omega\ cm^2$), while for $x = 0.1$ it is about 1 $\Omega\ cm^2$ and is remarkably greater. Although the electrical conductivity of the sintered samples increases by doping Mo (Fig. 5),

the increase of ASR for the sample with $x = 0.1$ can be due to the reduction of oxygen ion diffusion in the cathode. The obtained resistance values evaluated by fitting EIS data with EIS analyzer software are summarized in Table III. In this table, the ohmic resistance (R_Ω) corresponds to the electrolyte, electrode and current collector resistance. Charge transfer resistance (R_{ct}) is the high- and intermediate-frequency impedances related to the charge transfer process at the electrode/electrolyte interface. The non-charge transfer resistance (R_{nct}) is attributed to adsorption of oxygen and dissociation of O_2 into O^{2-} at the cathode surface.[23] According to these data, oxygen adsorption and diffusion are both limited by Mo doping. However, ASR values of $La_{0.9}Sr_{1.1}Co_{1-x}Mo_xO_4$ are still high for SOFC applications in comparison with the values for $R - P$ materials based on $Cu,La_{0.7}Sr_{0.3}CuO_4$ (0.16 $\Omega\ cm^2$ at 700°C)[37] and $Mn,La_{0.6}Sr_{1.4}MnO_4$ (0.39 $\Omega\ cm^2$ at 800°C)[38] and also undoped $La_{0.9}Sr_{1.1}CoO_4$ (0.35 at 850°C).[39] However, ASR values can be improved by optimizing the microstructure and also using the

electrode composite with appropriate contents of cathode and electrolyte. For example, in the work by Rieu et al.,[40] the ASR value of La_2NiO_4 reduced from 6 Ω cm^2 to 0.11 Ω cm^2 by optimizing the microstructure. To the best of our knowledge, this is the first time that structural, electrical and electrochemical properties of Mo-doped $La_{0.9}Sr_{1.1}CoO_4$ have been studied. However, more experiments need to be done to improve the electrochemical properties of $La_{0.9}Sr_{1.1}Co_{1-x}Mo_xO_4$ for SOFC application.

CONCLUSION

Ruddlesden–Popper $La_{0.9}Sr_{1.1}Co_{1-x}Mo_xO_4$ (x = 0, 0.03, 0.07 and 0.1) samples were synthesized by a modified sol–gel method. All samples had a tetragonal single-phase structure, after calcination at 1100°C in air. It was found that by doping $La_{0.9}Sr_{1.1}CoO_4$ compound with Mo ions, the Co^{4+}/Co^{3+} ratio and Co^{4+}–O–Co^{3+} double-exchange interaction were reduced. These reductions led to the coexistence of both FM and AFM components, observed from VSM analysis at room temperature. The electrical conductivity of the sintered $La_{0.9}Sr_{1.1}Co_{1-x}Mo_xO_4$ ceramics was found to increase with increasing Mo doping content and up to 800°C, which can be due to electron hopping between $Mo^{5+}(t_{2g}^1)$ and $Co^{3+}(t_{2g}^5e_g^1)$ through $O^{2-}(2p)$ as Co^{3+}–O–Mo^{5+} double-exchange interaction. The electrochemical measurements of the symmetrical cell showed that the polarization resistance decreases with increasing the temperature. The value of ASR for the sample with x = 0 was obtained as 0.36 Ω cm^2 and changed to 0.35 Ω cm^2 for x = 0.03 and 1 Ω cm^2 for x = 0.1, at 850°C.

ACKNOWLEDGMENTS

CONFLICT OF INTEREST

The authors declare that they have no conflict of interest.

REFERENCES

1. Y. Wang, J. Cheng, Q. Jiang, J. Yang, and J. Gao, *J. Power Sour.* 196, 3104 (2011).
2. D.J. Brett, A. Atkinson, N.P. Brandon, and S.J. Skinner, *Chem. Soc. Rev.* 37, 1568 (2008).
3. A. Gómez-Pérez, M.T. Azcondo, M. Yuste, J.C. Pérez-Flores, N. Bonanos, F. Porcher, A. Muñoz-Noval, M. Hoelzel, F. García-Alvarado, and U. Amador, *J. Mater. Chem. A* 4, 3386 (2016).
4. Z. Zhang, Y. Zhu, Y. Zhong, W. Zhou, and Z. Shao, *Adv. Energy Mater.* 7, 1700242 (2017).
5. J. Cui, Y. Gong, R. Shao, S. Wang, J. Mao, M. Yang, W. Wang, and Q. Zhou, *J. Mater. Sci.: Mater. Electron.* 30, 5573 (2019).
6. I. Belenkaya, A. Matvienko, and A. Nemudry, *J. Mater. Chem. A* 3, 23240 (2015).
7. I. Belenkaya, A. Matvienko, and A. Nemudry, *J. Appl. Crystallogr.* 48, 179 (2015).
8. M. Popov, I. Starkov, S. Bychkov, and A. Nemudry, *J. Membr. Sci* 469, 88 (2014).
9. O. Savinskaya and A. Nemudry, *J. Membr. Sci* 459, 45 (2014).
10. S. Huang, S. Feng, Q. Lu, Y. Li, H. Wang, and C. Wang, *J. Power Sour.* 251, 357 (2014).
11. A. Aguadero, D. Pérez-Coll, J. Alonso, S. Skinner, and J. Kilner, *Chem. Mater.* 24, 2655 (2012).
12. J. Wang, T. Yang, L. Lei, and K. Huang, *J. Mater. Chem. A* 5, 8989 (2017).
13. V. Cascos and J. Alonso, *Materials* 9, 579 (2016).
14. V. Cascos, R. Martínez-Coronado, and J. Alonso, *Int. J. Hydrog. Energy* 39, 14349 (2014).
15. M. Li, M. Zhao, F. Li, W. Zhou, V.K. Peterson, X. Xu, Z. Shao, I. Gentle, and Z. Zhu, *Nat. Commun.* 8, 13990 (2017).
16. A. Demont, R. Sayers, M.A. Tsiamtsouri, S. Romani, P.A. Chater, H. Niu, C. Martí Gastaldo, Z. Xu, Z. Deng, and Y. Bréard, *J. Am. Chem. Soc* 135, 10114 (2013).
17. E. Shubnikova, O. Bragina, and A. Nemudry, *J. Ind. Eng. Chem.* 59, 242 (2018).
18. R. Martínez-Coronado, J. Alonso, and M. Fernández-Díaz, *J. Power Sour.* 258, 76 (2014).
19. S. Huang, Q. Lu, S. Feng, G. Li, and C. Wang, *Adv. Energy Mater* 1, 1094 (2011).
20. Y.-F. Sun, Y.-Q. Zhang, B. Hua, Y. Behnamian, J. Li, S.-H. Cui, J.-H. Li, and J.-L. Luo, *J. Power Sour.* 301, 237 (2016).
21. X. Li and Y. Li, *J. Mol. Catal. A Chem.* 386, 69 (2014).
22. T. Wei, Q. Zhang, Y.-H. Huang, and J.B. Goodenough, *J. Mater. Chem.* 22, 225 (2012).
23. T. Ghorbani-Moghadam, A. Kompany, M. Bagheri-Mohagheghi, and M.E. Abrishami, *J. Magn. Mag. Mater* 465, 768 (2018).
24. Z. Talaei, H. Salamati, and A. Pakzad, *Int. J. Hydrog. Energy* 35, 9401 (2010).
25. A. Pakzad, H. Salamati, P. Kameli, and Z. Talaei, *Int. J. Hydrog. Energy* 35, 9398 (2010).
26. S. Gómez, J. Gurauskis, V. Øygarden, D. Hotza, T. Grande, and K. Wiik, *Solid State Ion* 292, 38 (2016).
27. W. Lu, Y. Sun, R. Ang, X. Zhu, and W. Song, *Phys. Rev. B* 75, 014414 (2007).
28. M.V. Sandoval, C. Pirovano, E. Capoen, R. Jooris, F. Porcher, P. Roussel, and G.H. Gauthier, *Int. J. Hydrog. Energy* 42, 21930 (2017).
29. Y.S. Chung, T. Kim, T.H. Shin, H. Yoon, S. Park, N.M. Sammes, W.B. Kim, and J.S. Chung, *J. Mater. Chem. A* 5, 6437 (2017).
30. Y.-P. Wang, Q. Xu, D.-P. Huang, K. Zhao, M. Chen, and B.-H. Kim, *Int. J. Hydrog. Energy* 42, 6290 (2017).
31. L.V. Makhnach, V.V. Pankov, and P. Strobel, *Mater. Chem. Phys.* 111, 125 (2008).
32. P.I. Cowin, R. Lan, C.T. Petit, and S. Tao, *Mater. Chem. Phys.* 168, 50 (2015).
33. M. Itoh, I. Ohta, and Y. Inaguma, *Mater. Sci. Eng. B* 41, 55 (1996).
34. F. Riza and C. Ftikos, *J. Eur. Ceram. Soc.* 27, 571 (2007).
35. M. Stawarz and P.M. Nuckowski, *Materials* 13, 1745 (2020).
36. E.P. Murray and S.A. Barnett, *Solid State Ion.* 143(3–4), 265 (2001).
37. Q. Li, H. Zhao, L. Huo, L. Sun, X. Cheng, and J.-C. Grenier, *Electrochem. Commun.* 9, 1508 (2007).
38. S. Liping, H. Lihua, Z. Hui, L. Qiang, and C. Pijolat, *J. Power Sour.* 179, 96 (2008).
39. Y. Hu, Y. Bouffanais, L. Almar, A. Morata, A. Tarancon, and G. Dezanneau, *Int. J. Hydrog. Energy* 38, 3064 (2013).
40. M. Rieu, R. Sayers, M. Laguna-Bercero, S. Skinner, P. Lenormand, and F. Ansart, *J. Electrochem. Soc.* 157, B477 (2010).